UNIVERSITY *of York*

This is a repository copy of *Multi-device studies of pedestal physics and confinement in the I-mode regime*.

White Rose Research Online URL for this paper:
https://eprints.whiterose.ac.uk/id/eprint/133757/

Version: Accepted Version

Article:

White Rose
university consortium
Universities of Leeds, Sheffield & York

eprints@whiterose.ac.uk
https://eprints.whiterose.ac.uk/

Multi-device Studies of Pedestal Physics and Confinement in the I-mode Regime

A. E. Hubbard[1], T. Osborne[2], F. Ryter[3], M. Austin[4], L. Barrera Orte[3,a], R. M. Churchill[7],

I. Cziegler[5,b], M. Fenstermacher[6], R. Fischer[3], S. Gerhardt[7], R. Groebner[2], P. Gohil[2],

T. Happel[3], J. W. Hughes[1], A. Loarte[8], R. Maingi[7], P. Manz[3], A. Marinoni[1], E. S. Marmar[1],

R.M. McDermott[3], G. McKee[9], T. L. Rhodes[10], J.E. Rice[1], L. Schmitz[10], C. Theiler[11],

E. Viezzer[3], J. R. Walk[1], A. White[1], D. Whyte[1], S. Wolfe[1], E. Wolfrum[3], Z. Yan[9],

and the Alcator C-Mod, ASDEX Upgrade and DIII-D Teams

[1] Plasma Science and Fusion Center, Massachusetts Institute of Technology, Cambridge, MA, USA.

[2] General Atomics, PO Box 85608, San Diego, California 92186-5608, USA.

[3] Max-Planck-Institut für Plasmaphysik, Boltzmannstraße 2, D-85748 Garching, Germany.

[4] Institute for Fusion Studies, University of Texas, Texas 78712, USA.

[5] University of California San Diego, Center for Momentum Transport and Flow Organization, La Jolla, California, USA.

[6] Lawrence Livermore National Laboratory, 7000 East Avenue, Livermore, California 94550, USA.

[7] Princeton Plasma Physics Laboratory, P.O. Box 451, Princeton, New Jersey 08543-0451, USA.

[8] ITER Organization, Route de Vinon-sur-Verdon, CS 90 046, 13067 St Paul Lez Durance Cedex, France.

[9] University of Wisconsin-Madison, Madison, Wisconsin 53706, USA.

[10] University of California Los Angeles, P.O. Box 957099, Los Angeles, California 90095-7099, USA.

[11] Ecole Polytechnique Fédérale de Lausanne (EPFL), Swiss Plasma Center (SPC), CH-1015 Lausanne, Switzerland.

E-mail contact of main author: hubbard@psfc.mit.edu

Abstract. This paper describes joint ITPA studies of the I-mode regime, which features an edge thermal barrier together with L-mode-like particle and impurity transport and no Edge Localized Modes (ELMs). The regime has been demonstrated on the Alcator C-Mod, ASDEX Upgrade and DIII-D tokamaks, over a wide range of device parameters and pedestal conditions. Dimensionless parameters at the pedestal show overlap across devices and extend

---

[a] Present affiliation: ITER Physics Department, EUROfusion - Programme Management Unit, Boltzmannstrasse 2, 85748 Garching.Germany

[b] Present affiliation: Department of Physics, University of York, York, UK.

to low collisionality.   When they are matched, pedestal temperature profiles are also similar.
Pedestals are stable to peeling ballooning modes, consistent with lack of ELMs.   Access to I-
mode is independent of heating method (neutral beam injection, Ion Cyclotron and/or
Electron Cyclotron Resonance Heating).   Normalized energy confinement $H_{98,y2} \geq 1$ has been
achieved for a range of $3 \leq q_{95} \leq 4.9$ and scales favourably with power.   Changes in turbulence
in the pedestal region accompany the transition from L-mode to I-mode.   The L-I threshold
increases with plasma density and current, and with device size, but has a weak dependence
on toroidal magnetic field B_T.   The upper limit of power for I-modes, which is set by I-H
transitions, increases with B_T and the power range is largest on Alcator C-Mod at $B > 5$ T.
Issues for extrapolation to ITER and other future fusion devices are discussed.

1. Introduction

I-mode is a promising regime that combines H-mode-like energy confinement with L-mode-
like particle and impurity transport, and without Edge Localized Modes (ELMs) [1].   The
key defining feature of the regime is the appearance of an edge temperature pedestal, similar
to that in H-mode, while the edge density profile remains similar to that in L-mode.   Hence,
particle and thermal transport are decoupled, an important feature for studying pedestal
physics.   High particle transport has a number of potentially important advantages for fusion
energy.   Intrinsic impurity and radiation levels are lower and do not build up over time,
which is particularly important with high Z Plasma Facing Component (PFC) materials such
as tungsten [2].   In fusion reactors, impurity seeding will be required to reduce divertor heat
loads, and high impurity transport should reduce impact of the introduced gasses on pedestal
and core confinement.   Particle transport will also be needed to remove helium 'ash'
produced by fusion reactions.   Without a particle barrier, plasma densities can also be more
readily controlled by fueling or pumping, important for burn control [3].   Another critical
advantage over H-mode is that the regime is naturally ELM-free, giving stationary conditions
for many energy confinement times τ_E without the need for active means to suppress ELMs.
It is now generally recognized that large ELMs will not be acceptable even in ITER, due to
heat pulses which erode the divertor [4].   While active mitigation methods including pellets
and magnetic perturbations exist, they are complicated to implement and there is concern

about degradation of the pedestal and resulting fusion performance. These issues will be even more serious for a reactor; hence development and exploration of intrinsically ELM-free regimes, including I-mode and alternatives such as Quiescent H-mode [5] are important.

Key to the potential extrapolation of the I-mode regime to ITER and future reactors is the scaling of accessibility conditions and performance. The multi-machine experiments reported here, supported by the Pedestal and Edge Physics as well as Transport and Confinement topical groups of the International Tokamak Physics Activity (ITPA), are the start of such studies. The regime has been most extensively studied in Alcator C-Mod but has also been explored for several years in ASDEX Upgrade [6]. More recently, I-mode has been observed on DIII-D [7]. Experiments on EAST, KSTAR, TCV and NSTX-U are planned soon, and this study aims to guide the choice of initial experimental parameters. Observations on the different devices share some general characteristics, but also reveal some differences.

This paper describes the experience and typical observations of the I-mode regime in each device, including density, temperature and electric field profiles and measured fluctuations in the transport barrier or 'pedestal' region (Section 2). In Section 3, we compare the operational spaces in which the regime has been observed to date, in terms of both global and pedestal parameters and energy confinement. Comparison of pedestal profiles in a dedicated identity experiment between C-Mod and AUG, shown in Section 4, provides further evidence of common physics across devices. Initial studies of power thresholds for accessing and remaining in I-mode are presented in Section 5. Section 6 discusses prospects and key open issues for extrapolation to future devices, including ITER.

2. Observations of the I-mode Regime in Tokamaks

The common means of accessing I-mode in tokamaks is to operate with 'unfavourable' ion $\mathbf{B} \times \nabla \mathbf{B}$ drift, away from the active X-point, and to increase the input power such that it remains below the H-mode threshold P(L-H), which is higher in this configuration. All discharges used in this paper are in this configuration and feature D as the main ion species, though some observations have been made in the favourable $\mathbf{B} \times \nabla \mathbf{B}$ configuration [8] and using H [6].

The I-mode regime and time of transitions are identified using the primary defining characteristics, namely

1) The formation of an edge temperature pedestal, i.e. a locally increased gradient, either abruptly or gradually, without a significant change in edge density profile with respect to L-mode.

2) Changes in edge turbulence, indicative of a change in local transport in the vicinity of the pedestal.

Signatures of an L-H-mode transition, namely an abrupt increase of density and drop in D_α, should be absent.   As will be described for each experiment below, I-mode discharges on Alcator C-Mod, ASDEX-Upgrade and DIII-D each share these characteristics.   There are, as may be expected, differences in the degree of these changes with plasma parameters, and some other features which have been observed to be typically associated with the regime.

2.1.   Alcator C-Mod

The I-mode regime has been most extensively and routinely studied in the Alcator C-Mod tokamak, a compact, high magnetic field device with Mo PFCs, major radius R=0.68 m, minor radius a=0.21 m and elongation κ~1.6-1.7.   Heating has been from Ion Cyclotron Resonance Heating (ICRH), with up to 5 MW coupled. Both reversed field, lower single null (LSN) and normal field upper null (USN) configurations have been used; in each case $\mathbf{B} \times \nabla \mathbf{B}$ drift is away from the X-point.   LSN has provided best performance and widest operating space, perhaps due to the shaped lower divertor designed for high heat flux.   As reported in the IAEA Fusion Energy Conference 2012 [9], stationary I-mode plasmas with τ_E reaching or often exceeding the ITER $H_{98,y2}$ scaling have been demonstrated over a wide range of plasma conditions.   Experiments in 2014 have further extended the range of parameters and improved measurements.   The lower magnetic field range has been extended to 2.8 T and some examples of I-mode have been noted in earlier 8 T experiments with $D(He^3)$ ICRH. Further extensions, including I-modes up to 8 T and examples in near double null configurations were made in the recently completed 2015 campaign, but these data have not yet been included in the multidevice datasets reported here.

Figure 1 shows an example of a steady I-mode at 5.8 T and 1.1 MA, with ICRH power increased stepwise from 2.6 to 4.6 MW.   A clear L-I transition is seen early in the second

power step, when pedestal and core T_e strongly increase but there is no break in slope in density. T_e pedestals, measured by Edge Thomson Scattering and Electron Cyclotron Emission (ECE), can reach 1 keV (Figure 2), while pedestal density stays near L-mode. T_i pedestals, measured by Charge Exchange Recombination Spectroscopy (CXRS), are equal to T_e in terms of gradient and height and can be overlaid within alignment uncertainties. A radial electric field (E_r) well forms in the same location as the T_i pedestal [10]. The pressure pedestal width exceeds that obtained in ELMy H-modes modes at the same pedestal value of poloidal beta, and is in fact wider than the semi-empirical scaling utilized in the EPED1.0 model. While the width is of the same order as the poloidal ion gyroradius, no correlation with $\rho_{i,pol}$ is found [11]. Stability analysis confirms that the pedestal is well below the peeling-ballooning stability limit, consistent with the typical lack of ELMs [3]. The margin between the observed p_{ped} and the stability limit indicates room to increase pedestal and global performance further; the upper bound is set either by available heating power, at optimal configuration and density, or in some cases by transitions from I-mode to H-mode. Initial confinement scalings show total plasma stored energy, W, increasing nearly linearly with the product of power and plasma current, resulting in a weak power degradation of energy confinement, at most $\tau_E \sim P^{-0.28}$[11]. For comparison, the H-mode scaling $\tau_{98,y2}$ degrades much more strongly, with $P^{-0.69}$ [12]. Impurity confinement τ_{imp} is similar in level and scaling to that in L-mode, 15-30 ms for both Ca and Mo injected species, vs 0.1-1 s in H-mode [13].

On Alcator C-Mod, distinct changes in turbulence in the pedestal region are associated with the transition from L-mode to I-mode, making clear that the change in local transport indeed represents a different confinement regime. Broadband density and magnetic fluctuations in the pedestal decrease, in approximately the 50-150 kHz band, proportionally to the drop in effective pedestal conductivity χ_{eff} during the L-I transition [8]. At the same time, an increase in fluctuations at higher frequencies is usually observed, on density, temperature and/or magnetic turbulence, localized to the pedestal temperature gradient region. This feature has been termed the 'weakly coherent mode' (WCM). It is clearest in low q_{95}, high power discharges. The relative density perturbation $\delta n_e/n_e$ is ~10% while $\delta T_e/T_e \sim 2\%$, consistent with a greater role in particle than thermal transport [14]. A correlation between the WCM amplitude and particle transport has been observed [15]. In addition to the WCM

a fluctuating zonal flow at the Geodesic Acoustic Mode (GAM) frequency, typically 20 kHz, is observed in the pedestal region only in the I-mode regime [16]. An example of both turbulent features is shown in Figure 3. The narrow feature in v_θ is at the GAM frequency, while the broad density fluctuation in the bottom panel is the WCM. Energy is transferred between the WCM and the GAM, away from the peak WCM frequency. This process likely contributes to the broad frequency spectrum ($\delta f/f \sim 0.5$) of the WCM.

Reductions in the core n_e and T_e turbulence, by typically 10-30%, have also been observed at the L-I transition, consistent with the decrease in core thermal transport [17]. Nonlinear gyrokinetic simulations of I-mode [18] show that I-mode core ion temperature and electron temperature profiles are more stiff than L-mode core plasmas. Scans of the input ExB shear in GYRO simulations show that ExB shearing of turbulence is a stronger effect in the core of I-mode than L-mode, which can help explain why core turbulence levels are reduced in I-mode. The nonlinear simulations show that I-mode resembles H-mode plasmas with regards to marginal stability of ITG modes and temperature profile stiffness.

2.2 ASDEX Upgrade

ASDEX Upgrade (AUG) is a larger tokamak with R=1.65m, a~0.5m and typical κ~1.6. The device is equipped with neutral beam injection (NBI), electron cyclotron resonance heating (ECRH), as well as ICRH. In the experiments reported here, up to 5 MW NBI at 60 kV has been used. Since 2011, up to 3.2 MW of ECRH has been available using the second harmonic extraordinary mode scheme which provides pure electron heating, in the core for B_T around 2.5 T. For the reversed B_T LSN configuration, the current must now also be reversed. Since counter-I_p NBI can lead to strong impurity production, I-mode studies in this configuration mainly used ECRH only. For the typical B_T and I_p configuration, I-mode was accessed in upper single null and more NBI could also be used. The LSN configuration allowed lower density due to better pumping capability. An important result from AUG is that I-mode can be produced independent of heating method (NBI, ICRH or ECRH); the majority of discharges presented here used NBI, ECRH or a combination of the two. We report here on several experiments from the 2009-2013 campaigns, with W PFCs. Some of these discharges were specifically aimed to match dimensionless parameters of C-Mod I-modes, as discussed further in Section 4.

An example of an I-mode discharge on ASDEX Upgrade is shown in Figure 4(a). In this case pedestal temperatures and global confinement increase gradually, starting at about 3.8 s. $H_{98,y2}$ exceeds 1.0 by 4.1 s. However, a spontaneous transition to H-mode, as evidenced by sharp changes in density and D_α emission, occurs at 4.12 s. In other cases, such as the example in Figure 4(b), I-mode remains stationary for many energy confinement times [6]. Detailed measurements of n_e and T_e profiles in the pedestal and core are available from Thomson scattering, DCN interferometry, ECE and a lithium beam. T_i, rotation and E_r are measured using CXRS. Example profiles, with T_i close to T_e, are shown in Figure 5. Core T_e and T_i are also approximately equal in this scenario. With ECH, pedestals are similar but T_e exceeds T_i in the core. An E_r well also gradually develops in the region of the temperature and pressure pedestal, which is intermediate between L and H-mode [19,20].

Reflectometry measurements in the AUG pedestal region exhibit a density oscillation whose characteristics are very similar to the C-Mod WCM. The frequency is in the range 70 - 150 kHz with a bandwidth (fwhm) of about 50 kHz. The amplitude of the density fluctuations in this frequency range increases somewhat as the I-mode pedestal develops while the amplitude of the fluctuations outside of the WCM frequency band decreases, such that the peak becomes more visible. The mode appears in close relation with the L-I transition independently of the heating method and seems to require a minimum value of the pressure gradient. It should be noted that the WCM is very similar to the "edge MHD mode" found in RF heated L-mode discharges in AUG [21].

Recent studies with 'hopping reflectometry' and Doppler reflectometry have provided further details of the weakly coherent mode, and have also revealed its interactions with a low frequency GAM in the 10 kHz range [22]. An example of evolution of frequency spectra is shown in Figure 6. The mode is located at normalized poloidal flux $\rho_{pol} \approx 0.98$, close to the location of the steepest T_e gradient and the minimum of the E_r well. The WCM is modulated by the GAM, in a manner similar to that observed on C-Mod. In contrast to C-Mod, the GAM is also commonly observed in L-mode as well as I-mode. High frequency magnetic fluctuations are also seen which are attributed to the geodesic Alfvénic mode, at similar but not identical frequencies to the WCM.

The development of the I-mode pedestal is also accompanied, in this radial region, by an increase in the time-averaged perpendicular velocity of the density fluctuations, while the erratic variations of this quantity also become more pronounced as the pedestal develops. Although the background turbulence level decreases, intermittent strong turbulence events of short duration (~10 μs) are observed [20].

2.3 DIII-D

I-mode experiments on DIII-D (R=1.67 m, a=0.67, carbon PFCs) have used the lower single null, reversed B_T configuration. The plasma current was kept in its typical orientation. Most discharges used NBI, with variable modulation to scan the average input power. ECH, and different combinations of co and counter NBI, were also assessed in the most recent experiments. Toroidal magnetic field was 2.05 T. I_p was varied from 1-1.6 MA, giving q_{95}=3.3-5.2. Shaping was scanned from δ_L=0.37-0.72 and κ=1.62-1.72, with most parameter scans at a fixed δ_L=0.53, κ=1.7.

The time history of a typical discharge is shown in Figure 7. As NBI power is slightly increased, there is a gradual increase in pedestal T_e and T_i and clear formation of an edge T gradient. Stored energy and normalized confinement time also increase, while density and D_α emission change only slightly. At slightly higher NBI power, the discharge transitions to ELMy H-mode, with a strong increase in n_e. The discharge thus shows the key feature of I-mode, though it is less robust than on the other tokamaks. As on ASDEX Upgrade, transitions were similar with NBI heating and/or ECH. Pedestal profiles from a different example, with I_p=1.2 MA, q_{95}=4.3, are shown in Fig. 8. Density profiles in I-mode are very similar to L-mode, while T_e is intermediate between L-mode and H-mode. A difference from ASDEX Upgrade and C-Mod is that, in all regimes, pedestal ion temperatures are significantly higher than electron temperatures, indicating weak electron-ion coupling. Similar to C-Mod and AUG, E_r shear increases in the regions of the T_i pedestal, and is also intermediate between L-mode and H-mode levels [7].

Changes in fluctuations are also observed during the I-mode phase. The power spectrum of line-integrated n_e fluctuations on Phase Contrast Imaging (PCI) decreases, broadens, and

shows a weak minimum at f~ 200 kHz and a peak at 300-400 kHz [7]. Examples of PCI spectra are shown in Figure 9(a). Doppler back-scattering, which is also sensitive to n_e fluctuations [23], localizes the decrease to a region near the pedestal top (Fig 9(b)). The characteristics are intermediate between L-mode and H-mode turbulence, and evolve gradually during the period in which a T pedestal forms. Bursts of n_e and T_e fluctuations in the 60 kHz range have also been observed in some discharges, localized near the top of the T_e pedestal and accompanied by small increases in divertor D_α. An example is shown in Figure 10. This 'burstiness' in D_α can also be seen as an increased fluctuation level in the example of Fig. 7, and may indicate more intermittent transport in I-mode as seen on AUG. The instability causing these fluctuations is unclear. Similar to the C-Mod results [3], the pedestal ∇p in I-mode is low, more than a factor of 4 below the critical gradient for peeling-ballooning mode stability reached before the ELMs in the H-mode phase as computed with ELITE [24], and also roughly a factor of 2 below the ideal infinite-n ballooning mode limit. Hence the D_α bursts are not typical Type I ELMs. The lower pressure gradient, and the fact that the pedestal width in DIII-D I-mode is a factor of 2 to 5 larger than EPED1.0 scaling [25], as shown in Figure 11, also indicates that I-mode edge pressure gradient is not set by the kinetic ballooning mode as is thought to be the case in H-mode.

3. Comparison of achieved global and local parameters for I-mode.

An important task of this joint activity has been to assemble and compare a database of plasma parameters in achieved I-modes in each of the above devices. It should be noted that it is not exhaustive, in that experiments have not yet assessed all of the operating space in each tokamak. Rather it provides a map of where I-modes have been achieved to date and serves as a guide to potentially important parameters, and for extrapolation to other tokamaks.

I-mode has been obtained over a very wide range of plasma currents and magnetic fields: B_T 1.9 to 8 T, I_p 0.55 MA to 1.43 MA, and q_{95} from 2.4 to 5.3, as shown in Figure 12. The regime is thus clearly not restricted to a narrow operating point. Figure 12(b) shows that the bulk of the discharges are in the range q_{95} 3 to 4.2, the range planned for key ITER scenarios. Furthermore, on C-Mod and ASDEX Upgrade, normalized confinement $H_{98,y2}$ reaches or exceeds 1 across the range $3<q_{95}<4.9$. As can be seen, however, there is a wide range from $0.6<H_{98,y2}<1.3$, and the DIII-D discharges so far tend to be on the low end of the range, $H_{98,y2}$

up to 0.8. In both C-Mod and AUG, τ_E in I-mode does not degrade significantly with power as in H-mode [9,3,6,11], thus the best normalized and absolute performance is achieved when maximum power can be applied and pedestal pressures achieved.   This trend contrasts with the $\tau_E \sim P^{-0.7}$ scaling of $H_{98,y2}$.   Trends in pedestal pressure with power are similar, consistent with the peeling-ballooning stable pedestals noted in Section 2.   Global parameters for I-modes to date are summarized in Table 1.

	C-Mod	**AUG**	**DIII-D**
I_p (MA)	0.56-1.4	0.8-1.0	0.96-1.4
B_T (T)	2.8-8.0	1.9-2.5	2.04
q_{95}	2.4-5.2	3.0-4.1	3.5-5.2
$\bar{n}_e$ (10^{20} m^{-3})	0.9-2.3	0.16-0.3	0.22-0.51
$\bar{n}_e/n_G$	0.11-0.35	0.22-0.6	0.26-0.53
P_{loss} (MW)	1.5-5.1	1.6-3.0	2.4-4.1
Heating method	ICRH	NBI, ECH, ICRH	NBI, ECH

The three tokamaks also span an extremely wide range of pedestal parameters in I-mode, as shown in Figure 13(a). Alcator C-Mod has the absolute highest densities, up to $n_{e,ped}$=1.6x10^{20}m^{-3} ($\bar{n}_e$=2.3x10^{20}m^{-3}).   The range on DIII-D is lowest, $n_{e,ped}$=1.8-3.4x10^{19}m^{-3}, while ASDEX Upgrade tends to run at slightly higher densities (2.1-4.4x10^{19}m^{-3}), and reaches 60% of the Greenwald density limit.   For both AUG and C-Mod, electron T_{ped} is typically in the range 0.4-0.800 keV, with some C-Mod discharges reaching 1 keV; as noted previously, T_i pedestals are very similar.   On DIII-D $T_{e,ped}$ is notably lower, 0.2-0.400 keV.   However, in these mainly NBI heated discharges T_i pedestals, which are measured from CXRS and included for some discharges in this dataset, tend to be somewhat higher than T_e, up to ~0.6 keV at the same location.   This is seen also in the example of Figure 8.   The range of $T_{e,ped}$ for NBI and ECH-heated discharges on DIII-D was comparable, with T_i closer to T_e for ECH-dominated discharges.   The upper limit to T_{ped} in both AUG and DIII-D I-modes was set by the transition to H-mode at higher input power.   While this was also the case in some C-Mod discharges, in many others the maximum available heating, P_{loss} up to 5 MW and 3.5 times the

ITPA L-H threshold scaling (for favourable magnetic configuration), could be added without transitions, and T_{ped} and p_{ped} continued to increase with P_{loss}. The upper range of average pressure in I-modes is set by the same limitations of thresholds and power. To date, the maximum normalized pressure on all devices has been modest, up to $\beta_N=1.4$. However, there is not an apparent MHD limit encountered.

The devices show greater commonality in dimensionless pedestal parameters. Figure 13(b) shows pedestal gyroradius $\rho^*=\rho_i/a$, computed using $T_{e,ped}$, vs electron collisionality ν^*_{ped}, computed assuming $Z_{eff}=1.2$. A wide range is seen in both parameters, with $\nu^*_{ped}=0.17\text{-}4.3$, and $\rho^*=2.2\text{-}5.5\text{x}10^{-3}$. AUG pedestal data and the C-Mod pedestals at $B_T=4\text{-}6$ T have strong overlap; indeed some of the experiments were carried out with the aim of producing dimensionless matches as discussed in Section 4. Importantly for future devices, many of the high performance I-modes are at low ν^*, and there is no indication of a lower limit in collisionality or q_{95}. This contrasts with the operation spaces for 'grassy', Type II and Enhanced D-alpha (EDA) H-mode small or no ELM regimes as found in a prior ITPA study [26].

Due to the lack of a particle barrier, natural density ranges in I-mode tend to be lower than in H-mode. Above a certain target density, discharges typically transition directly from L-mode to H-mode. However, C-Mod has demonstrated that the density can be increased by fueling after the transition to I-mode [9]. With sufficient input power, T_{ped} can be maintained [3]. The limits in density, as for pressure, are generally set by I-H transitions. The I-mode operating space is thus dependent on transition physics and scalings, the subject of Section 5.

4. Dimensionless identity experiment between AUG and C-Mod

A well-known approach for comparisons between different devices consists in performing so-called dimensionless identity experiments in which the plasmas are designed such that the dimensionless plasma quantities (ρ^*, ν^*, β ...) take the same values in the devices, see e.g. reviews [27,28,29]. If the match over the whole radius is perfect, $B_T\tau_E$, where τ_E is the global energy confinement time, also has the same value in the two devices, in this case AUG

and C-Mod . In the frame of the ITPA TC-18 joint experiment, this method has been applied for I-modes in, and the emphasis was put on the identity in the pedestal region. In this approach, the following scaling rules are applied to obtain the identity of the plasma parameters: $B_T \sim R^{-5/4}$, $I_P \sim R^{-1/4}$, $n_e \sim R^{-2}$ and $T \sim R^{-1/2}$, which for equivalent confinement, constant, should require $P_{loss} \sim R^{-3/4}$. In addition q_{95}, plasma shape, heat deposition profiles should be kept as similar as possible. A similar approach has proven valuable for multidevice comparisons of H-mode pedestals and L-H transitions, eg [30].

Close but not exact matches of these parameters, and of shape, were achieved in these experiments, with magnetic field and density 5.8 T and 1.5×10^{20} m^{-3} on C-Mod and 1.9 T and 0.25×10^{20} m^{-3} on AUG. As shown by Figures 15(a) and (b), the density in C-Mod is at the upper boundary of the I-mode domain, whereas it is at the low boundary for AUG, limiting somewhat the flexibility in these experiments. The plasma gas was deuterium and in both cases the ion $\mathbf{B} \times \nabla \mathbf{B}$ drift was away from the active X-point as required for reliable I-modes. In C-Mod the heating method was ICRH hydrogen minority, while in AUG NBI was used with in addition about 20% of central ECRH to prevent any risk of tungsten accumulation. This leads to dominant electron heating in the central part, $q_e/q_i > 1.4$ for $\rho_{tor} < 0.5$, while $q_e \approx q_i$ at the plasma edge, as revealed by the power balance calculations.

The pedestal temperature profiles in a developed I-mode for the best match obtained in the two tokamaks are shown in Figure 14(a). The AUG profile has been scaled to C-Mod according to $T \sim R^{-1/2}$. In C-Mod the profile is provided by Thomson scattering. In AUG the T_e profile is deduced from the ECE radiation temperature using a forward modelling to compute the actual thermal temperature [31]. The T_i profile, also measured in AUG with the CXRS systems but not shown here, is very similar to T_e in the pedestal region but is significantly lower in the core due to the rather high ratio of central electron to ion heating. The density profile in AUG is obtained by combining the edge measurement from the Li-beam with the line-integrated data of the DCN interferometer and by Thomson scattering in C-Mod. Some differences in density profiles (Figure 14(b)) are seen, with higher separatrix densities on C-Mod and profiles shifted outward. Such differences have also been found in density profiles in H-mode identity experiments between C-Mod and the larger, lower B

tokamaks DIII-D[32] and JET[33], likely reflecting the influence of particle sources; ionization lengths are influenced by atomic physics and are shorter at high absolute density.

Despite the good match in the pedestal, the $B_T\tau_E$ values differ significantly with $B_T\tau_E = 0.266$ in C-Mod and $B_T\tau_E = 0.173\pm0.02$ [T s] in AUG. The loss power is 2.9 MW in C-Mod and 1.8 MW in AUG, which would correspond to a scaled value of 3.5 MW. Considering the good agreement in the pedestal, this difference $B_T\tau_E$ most likely arises from the core, whereby a possible explanation for the lower value in AUG can be the high T_e/T_i ratio in the central part of the plasma, linked to the higher local electron heat flux mentioned above. Indeed $T_e/T_i >$ 1.5 for $\rho_{tor} < 0.5$ such that the ion energy content contributes to only one third of the total plasma energy content. In addition, the heating methods and profiles were different, with a more peaked central deposition on C-Mod; uncertainties in ICRH absorption could also contribute to the differences in P_{loss} and τ_E.

We also observed that, in the matched density cases, the scaled threshold power, P(L-I) and edge temperature, and the increase of T_{ped} with P_{loss}, were also very similar between C-Mod and AUG. Thus, despite some differences in the core, these results indicate that the I-mode threshold and pedestal physics are indeed similar across devices.

5. Power thresholds for L-I and I-H transitions.

To be attractive as a regime for fusion, I-mode must be accessible at a reasonably low power, and also be maintained, without transitions to H-mode or back transitions to L-mode, for a sufficiently high power and at high enough density to reach high fusion power. Studying thresholds for both L-I and I-H transitions is thus important. To this end, we have analysed in addition to time slices within the I-mode phase, powers and parameters just before the transitions, denoted as threshold conditions. We define $P_{loss}=P_{oh}+P_{heat}$(absorbed)$-dW/dt$, where P_{oh} is the ohmic power, P_{heat} is the auxiliary power (ICRH, NBI and/or ECH) and W the stored energy. For AUG and DIII-D, only thermal contributions to W are included.

For a given current, magnetic field and configuration, the L-I power threshold scales at least linearly with density on both C-Mod and AUG [34]. An example from Alcator C-Mod, for

LSN discharges with B_T 5-6 T and I_p 1-1.1 MA, is shown in Figure 15(a). An increase in P_{L-I} is seen below a certain lower density, as is typical for L-H thresholds.   AUG observes an offset linear dependence of P_{L-I} with n_e, as shown in Figure 15(b) which includes all conditions.   L-I transitions on DIII-D, in contrast, do not show a clear density dependence (Fig. 15(c)).   It should be noted that transitions from L-mode to I-mode on DIII-D tend to be very gradual, as shown in Figure 7, and it can be difficult to pinpoint an exact time from profile measurements alone, hence the L-I "thresholds" give an approximate indication of the lower range of power in I-mode.   However, the lack of an increase in power with density suggests that many of these discharges were at densities below the minimum threshold.   The range of power for given density is relatively narrow, typically 2 MW.

I-H power thresholds are much more variable.   On C-Mod, at high L-mode target density, prompt H-mode transitions can occur at moderate power.   Such a case is included in Fig. 15 (a) (black open triangle).   However, by increasing power and density together, the range of each can be significantly increased [9].   In this high density I-mode regime, I-H transitions can sometimes be triggered by a *decrease* in heating power.   These results suggest a possible limit in collisionality, which should be explored further,   For AUG also, I-H thresholds are scattered and at high density can even be at lower P_{loss} than L-I transitions.   Thus, a simple power scaling does not seem to capture all the relevant physics of I-H transitions.   On DIII-D, I-H transitions do occur at the upper range of power, but P(I-H) exhibits an inverse dependence on density, again suggesting the experiments were in a density regime below the minimum threshold for I-mode.   I-mode formation did not depend strongly on heating method (ECH vs NBI) in either AUG or DIII-D.   A torque scan was conducted on DIII-D to vary E_r and E×B velocity shear.   Discharges showed a modest reduction in the I-H transition power with balanced NBI injection while with ECH the threshold was similar to the co-NBI injection cases; these trends are similar to those for L-H threshold power on DIII-D [35].

Since the I-H power threshold is poorly defined, for size scaling comparisons between devices we use the L-I threshold and the observed power range in I-mode.   C-Mod also observes an increase in the L-I power threshold with current [34]. To reduce this dependence, which is not seen in L-H threshold scalings [36], we restrict to discharges with $3<q_{95}<4.4$. P_{loss} is normalized by line average density, omitting the lowest density discharges for which L-I thresholds are increasing.   Comparing P(L-I)/n_e on C-Mod (S~7 m^2), AUG (S~44 m^2), and

DIII-D (S~52 m^2) we find the size dependence at most linear with surface area S, as shown in Figure 16. Given the variation in the dataset, somewhat weaker dependences, such as S$^{0.7}$ (dotted curve) would also be consistent. Noting the differences in plasma parameters between devices, further experiments on other tokamaks will help to clarify such dependences.

An experiment was carried out on C-Mod to assess the toroidal field dependence of the power range in I-mode. Discharges at 2.8 T, 550 kA, at the same shape and q$_{95}$ as the example shown in Figure 1, and the dataset in Figure 15(a), were heated using 2nd harmonic H minority ICRH. The observed power and density ranges for I-mode were much lower; L-I transitions occurred with 1.2 MW ICRF (P$_{loss}$=1.46 MW), at $\bar{n}_e$ = 1.04x10^{20}m^{-3}, while discharges transitioned to H-mode at only 1.5 MW (P$_{loss}$=1.54). This very narrow (5%) power range contrasts strongly with the much wider range, more than a factor of two, seen at 5.6 T. It is closer to that observed on DIII-D and AUG. Figure 17 shows normalized power P$_{loss}$/$\bar{n}_e$S vs B$_T$. As for Figure 16, we have restricted to 3<q$_{95}$<4.4 and densities above the minimum P(L-I). We note that C-Mod magnetic field ranges other than 4-6 T use heating scenarios which may have lower absorption than assumed here, hence powers are an upper bound. For both C-Mod and the combined dataset, it appears that the lower bound of L-I thresholds has a weak dependence on B$_T$; a value of P/$\bar{n}_e$S=0.15-0.25x10^{-20}MWm (shaded band on Fig. 17) is consistent with many of the transitions on all three devices. For comparison the latest ITPA threshold scaling is P(L-H)= $\bar{n}_e$$^{0.72}B^{0.80}S^{0.94}$ [36]. The upper bound of I-mode powers increases strongly with B$_T$; we note that many of the discharges at > 5 T are limited by available heating power and that the upper line does not necessarily reflect an I-H threshold. While more experiments are required to confirm this trend of increasing power range for I-mode with higher B$_T$, and to understand the underlying physics, which may not depend simply on the value of B$_T$, it is consistent with the different experience in terms of robustness of the regime on C-Mod (at B > 5 T) to that at DIII-D and ASDEX Upgrade. Experiments to study I-mode at 8 T were conducted very recently on C-Mod and are consistent with these trends and B$_T$ scaling is also being extended on AUG; details will be reported separately.

6. Conclusions and implications for future experiments.

The multi-machine studies in this paper have shown that the I-mode regime can be achieved in the 'unfavourable' ion $\mathbf{B}\times\nabla\mathbf{B}$ drift configuration over a very wide range of global and local parameters (B_T=1.9-8 T, I_p=0.55-1.4 MA), and with multiple heating methods (ICRH, ECRH and NBI). The main features of I-mode are common to Alcator C-Mod, ASDEX Upgrade and DIII-D and include:

- formation of ion and electron temperature pedestals,
- increase in stored energy,
- little or no change in density,
- E_r well developing in T pedestal region, intermediate between L-mode and H-mode,
- usually no ELMs.

Similar changes in pedestal turbulence are also seen in each device. While details differ, each sees a reduction in part of the spectrum, and a peak in density fluctuations at higher frequency. A fluctuating flow at the GAM frequency also plays a role, strongly interacting with the Weakly Coherent Mode on both AUG and C-Mod. Greater intermittency in turbulence is also observed; this has been most carefully studied on AUG.

The L-mode like particle transport found in the I-mode regime is advantageous for fusion in several respects, avoiding impurity accumulation and providing steady, readily controllable densities and compatibility with impurity seeding to reduce divertor heat fluxes. Notably, both C-Mod and AUG operate with high Z plasma facing components (Mo and W, respectively). The three devices span a wide range of pedestal n_e and T_e, and also ν_*, q_{95} and ρ_*. Importantly for extrapolation to burning plasmas, there is no indication of a lower limit in any of these dimensionless parameters. Pedestals are MHD stable, consistent with the lack of ELMs. Energy confinement exceeding H-mode scalings has been observed over a wide range of q_{95} on both C-Mod and ASDEX Upgrade. A next step in this joint ITPA activity will be to extend the dataset and attempt a new confinement scaling for I-mode which better captures the power dependence, which appears more favourable than H-mode, and other parameter dependences. New experiments planned soon on EAST, KSTAR, NSTX-U and TCV should offer additional data. Results from JET would be valuable in extending the size scaling.

Perhaps the most important issue for I-mode concerns the threshold conditions to access the regime, and to maintain it without transitions to H-mode. Both C-Mod and AUG find P(L-I) increasing with density. C-Mod results show a scaling with plasma current. From the multi-machine dataset, the size scaling is at most linear with surface area. A threshold of $P_{loss}/\bar{n}_e S$=1.5-2.5x10^{-21}MW m fits most of the current observations on all three tokamaks.

The power range for which I-mode can be maintained differs between devices. Recent C-Mod experiments, and our multi-machine dataset, indicate that this is due to different toroidal magnetic field; L-I thresholds have a weak dependence on B_T, while the upper range in power increases strongly with B_T. The result is encouraging for ITER, which will also operate at 5.3 T, and implies that I-mode may be especially well suited to even higher magnetic field tokamaks such as have been proposed for future compact fusion devices [37,38]. For ITER, with S=678 m^2, this would imply an L-I threshold of 68 MW at $\bar{n}_e$=5x10^{19}m^{-3} for deuterium plasmas, which is somewhat larger than the expected H-mode threshold for the favourable B_T direction of 52 MW for deuterium plasmas (42 MW for DT). If size scaling is weaker, as could also be consistent with the data, or the L-I threshold with DT is reduced compared to deuterium plasmas as is the case for the L-H threshold, the required power could be much lower.

Another open and important issue under study is the extent to which density can be increased, along with total heating and fusion power, while remaining in I-mode. The observed upper range for I-modes of $P_{loss}/\bar{n}_e S \leq$ 5x10^{-21} MW m at 5.4 T would correspond to $P_{loss} \leq$350 MW for ITER at $\bar{n}_e$=10^{20}m^{-3}. This is well above the expected auxiliary + alpha power power in the typical high Q_{DT} operational scenarios in ITER ($P_{loss} \leq$ 150 MW), hence it should be possible to stay in I-mode. A related issue, important for extrapolation to steady state reactors, is how high a normalized pressure, β or β_N, can be achieved in I-modes. In general, the physics and scaling of I-H transitions and thresholds requires further study.

In order to operate with unfavourable drifts, ITER would need to reverse the direction of the plasma current as well as B_T, to keep the same edge magnetic field helicity which is required because of the design of plasma facing components for optimum power handling. Operation

in reversed I_p-B_T has operational requirements that cannot be met by the NBI injection system planned in ITER; therefore ICRH and ECRH are foreseen to be the heating schemes to be applied if the I-mode regime is investigated in ITER. Future new fusion facilities planning to exploit the I-mode regime should design for flexibility in magnetic drift direction. Further studies on our present devices will extend the studies of transitions, and physics underlying them, including fluctuations and flows in the pedestal region.

Acknowledgements

Figures

FIG. 1: *Stationary high confinement I-mode discharge on Alcator C-Mod (Pulse 1120907028, 5.8 T, 1.1 MA, LSN). Early in the second step of ICRF power (a), core T_e (c), pedestal T_e (d) and plasma pressure (e), approximately double, indicating the transition from L-mode to I-mode. Density (b) and D_α emission (g) remain at L-mode levels. Normalized energy confinement $H_{ITER98y2}$ (f) increases from 0.6 to 1.2.*

Fig 2
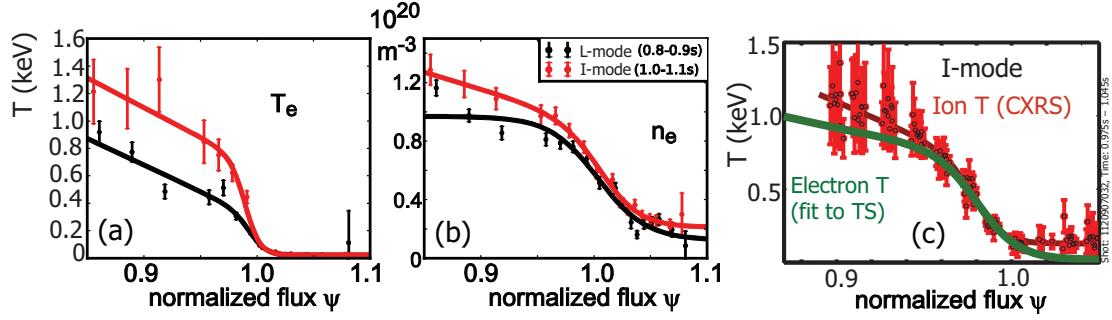
FIG 2. Electron temperature (a) and density (b) profiles for the discharge of Figure 1, in I-mode (red) and L-mode (black) phases. (c) Pedestal T_i in I-mode (red) measured for a slightly higher density discharge (1140907032) in the same experiment, is equal to T_e (green) within relative alignment uncertainties.

Fig 3:
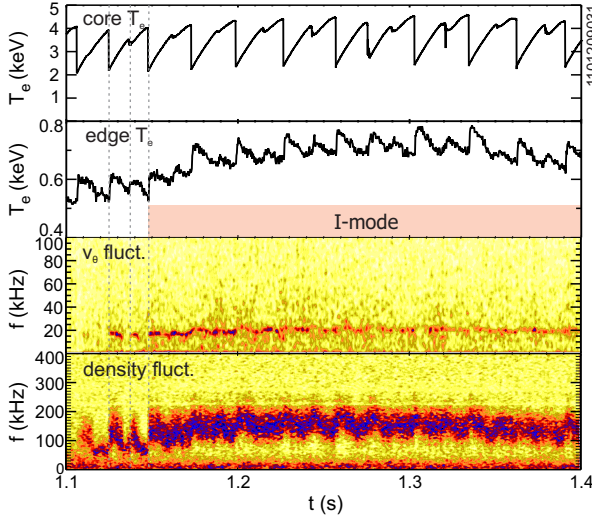
FIG 3. Time history of a long lived I-mode discharge, Traces are, from top, core electron temperature, pedestal electron temperature at the top of the pedestal, spectrogram of the poloidal velocity $\sim v_\theta$ from edge Gas Puff Imaging spectrogram of GPI, and density fluctuations in the same spatial location, restricted to a wavenumber range $0.5\ cm^{-1} < k_\theta < 2.0\ cm^{-1}$ to highlight the WCM. From Cziegler [16].

Fig 4.
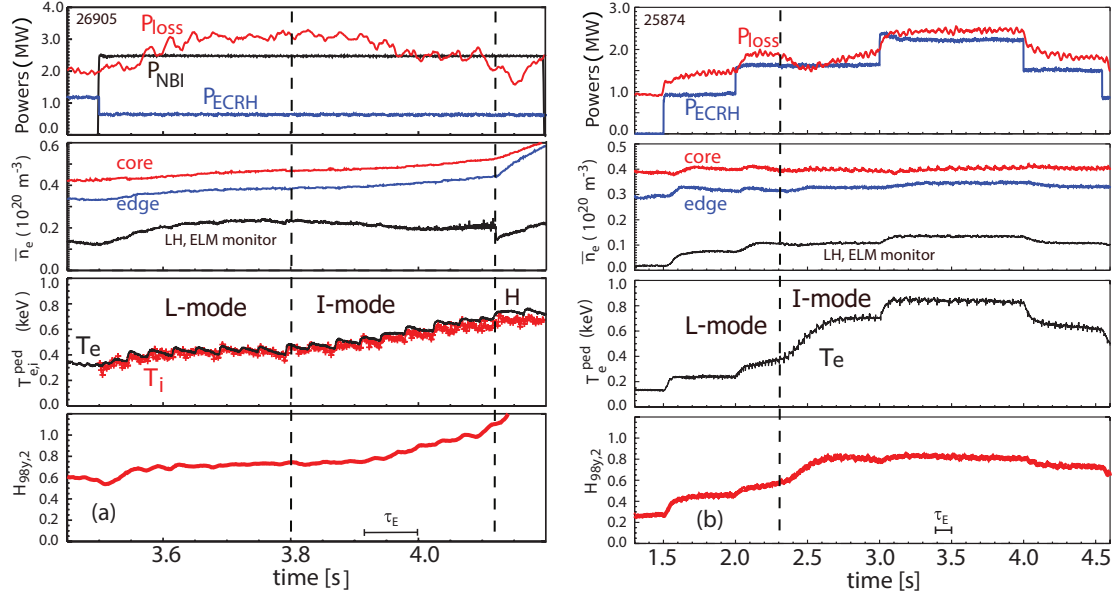
FIG 4(a). Time traces from an I-mode discharge (26905) on ASDEX Upgrade. In this case the pedestal evolves slowly and there is a transition to H-mode. (b) Example of an I-mode phase which after initial slow evolution continues until the end of the heating, over 20 confinement times (25874). Traces show, from top, heating powers, core and edge density, pedestal temperatures, and normalized confinement H_{98y2}. Other parameters are quite similar (0.99 MA, 2.5 and 2.3 T respectively) in the two discharges.

Fig 5
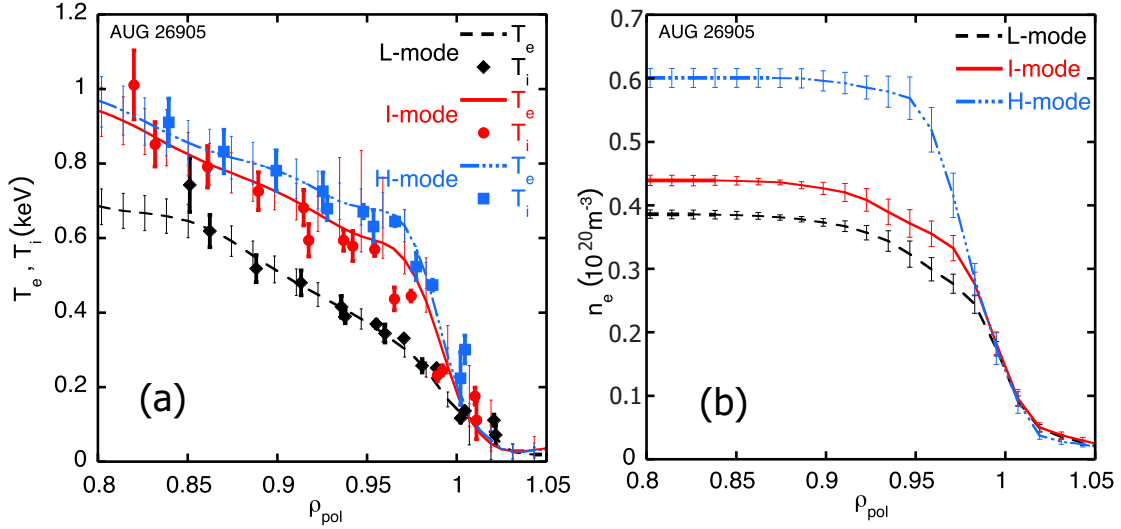
FIG. 5. Pedestal T_e and T_i profiles (a) and electron density profiles (b) in the same AUG discharge as Fig. 4(a). Temperatures in I-mode (red) are higher and steeper than in L-mode (black). Density profiles in I and L-mode are very similar, and as usual increase sharply in H-mode (blue).

Fig 6.
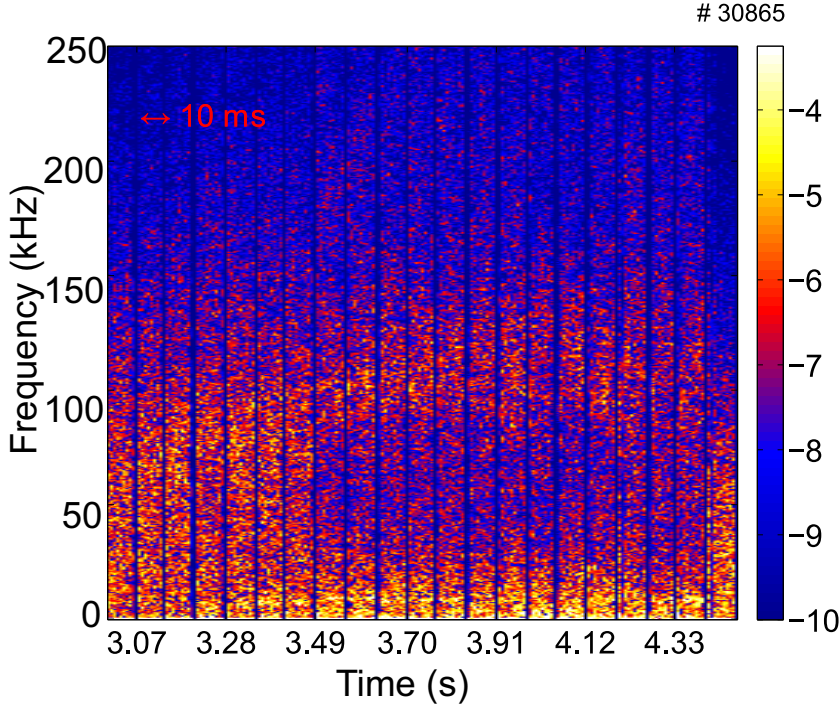
FIG. 6. Density fluctuation spectra measured by hopping reflectometry. As the I-mode develops (3.4-4.3 s), turbulence reduces below 100 kHz and the Weakly Coherent Mode develops at about 120 kHz. From Manz et al [22]

Fig 7
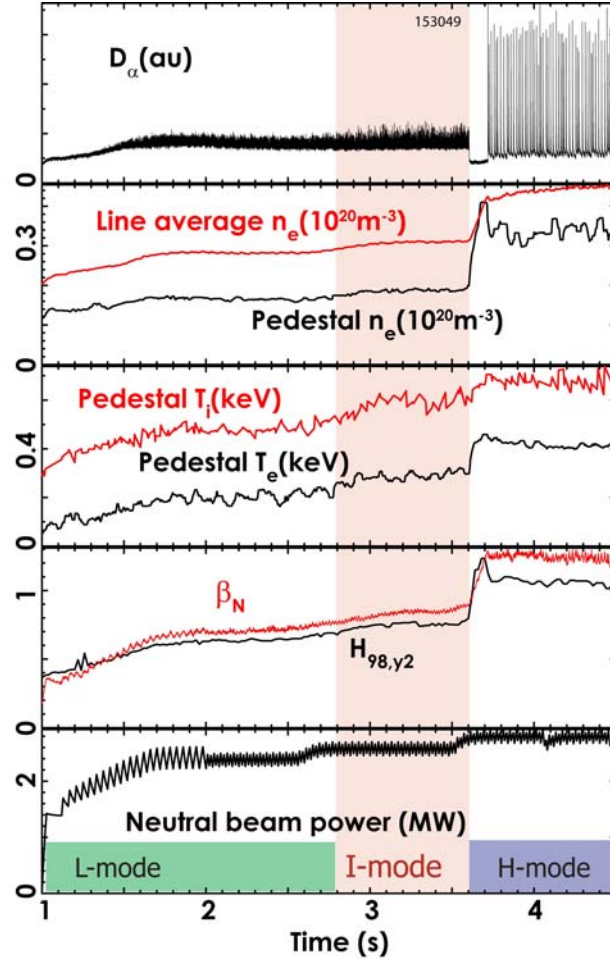
FIG. 7: Time evolution of a neutral-beam heated I-mode discharge (153049) on DIII-D (0.98 MA, 2.05 T, q_{95}=5.1).

Fig 8
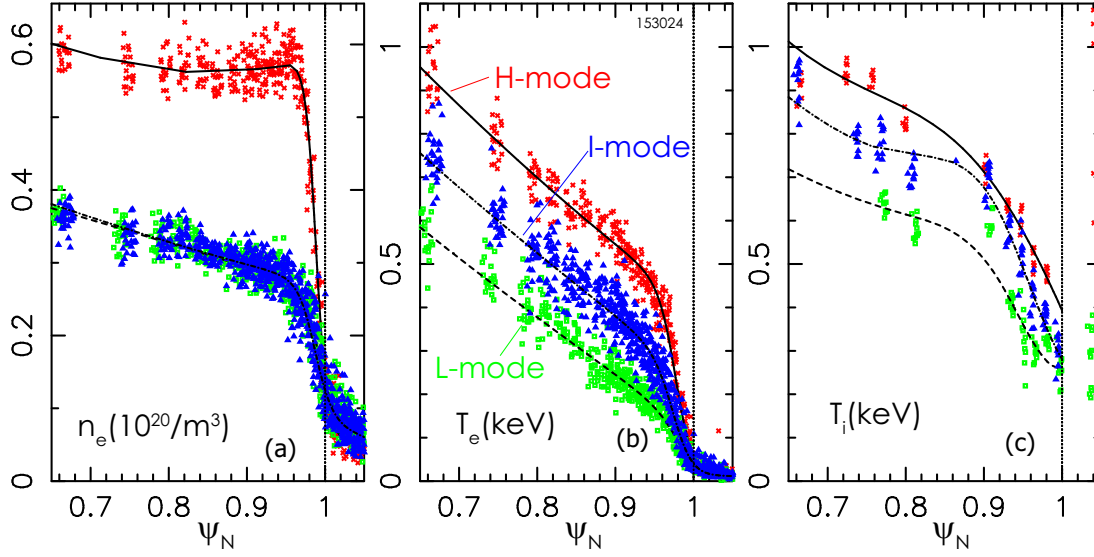
FIG. 8: Pedestal profiles of (a) electron density (b) electron temperature and (c) ion temperature in different regimes for a DIII-D discharge 153024, with up to 3 MW neutral-beam heating D (1.2 MA, 2.05 T, q_{95}=4.3).
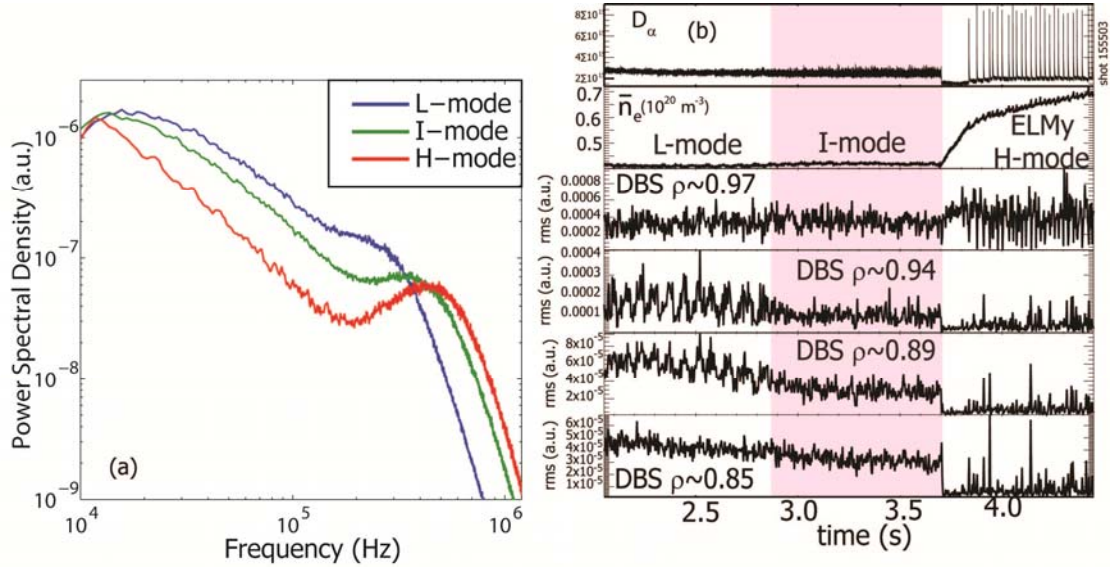
Fig 9

FIG. 9(a).   Power spectral density measured by Phase Contrast Imaging, for DIII-D discharge 153031.   (b) Time dependence of n_e fluctuations from Doppler Backscattering for discharge 155503 (2.05 T, 1.2 MA, $\bar{n}_e = 5 \times 10^{19} m^{-3}$), showing a gradual decrease in mean amplitude in I-mode which is localized to $\rho = 0.89$-0.94.   Adapted from [7]

Fig 10
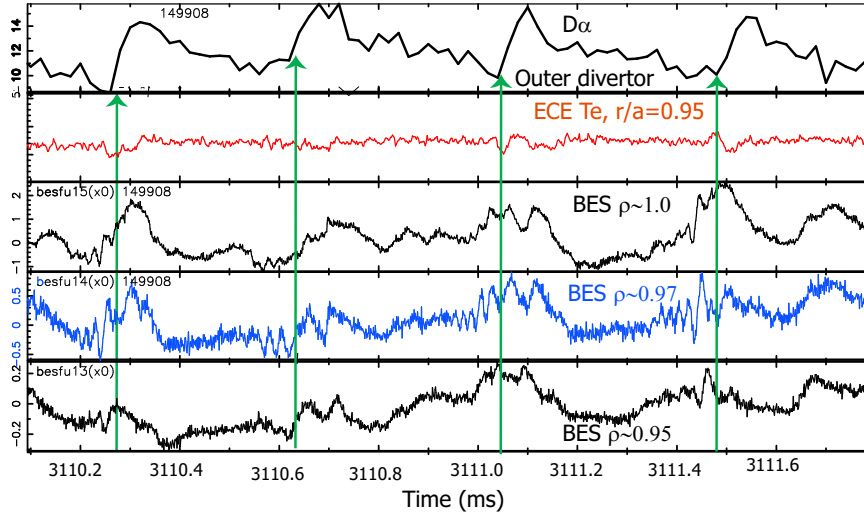
FIG. 10. *Details of D$_\alpha$ emission (top), T$_e$ fluctuations from Electron Cyclotron Emission (second trace) and density fluctuations, from Beam Emission Spectroscopy during an I-mode period on DIII-D discharge 149908 (1.2 MA, 2.05 T). Periodic bursts of fluctuations are seen which result in small increases in D$_\alpha$, indicating increased particle transport.*
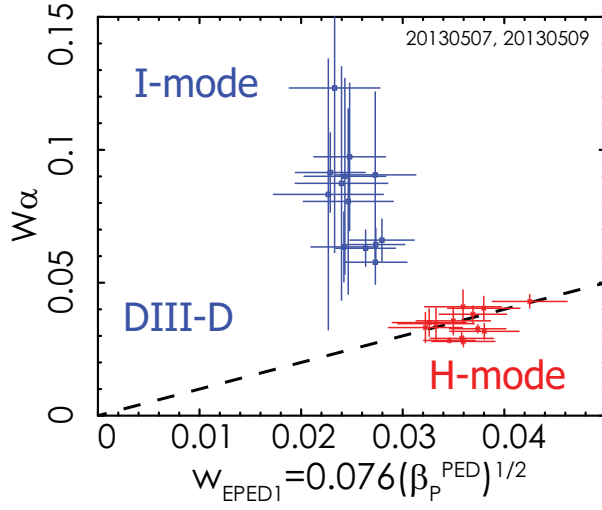
Fig 11

FIG. 11: *Width of DIII-D pressure pedestal vs prediction of EPED1 model, using the measured pedestal pressure, for some recent I-mode and H-mode experiments. H-mode time slices (red) agree with predictions as expected, while I-modes (blue) are significantly wider indicating different controlling physics.*
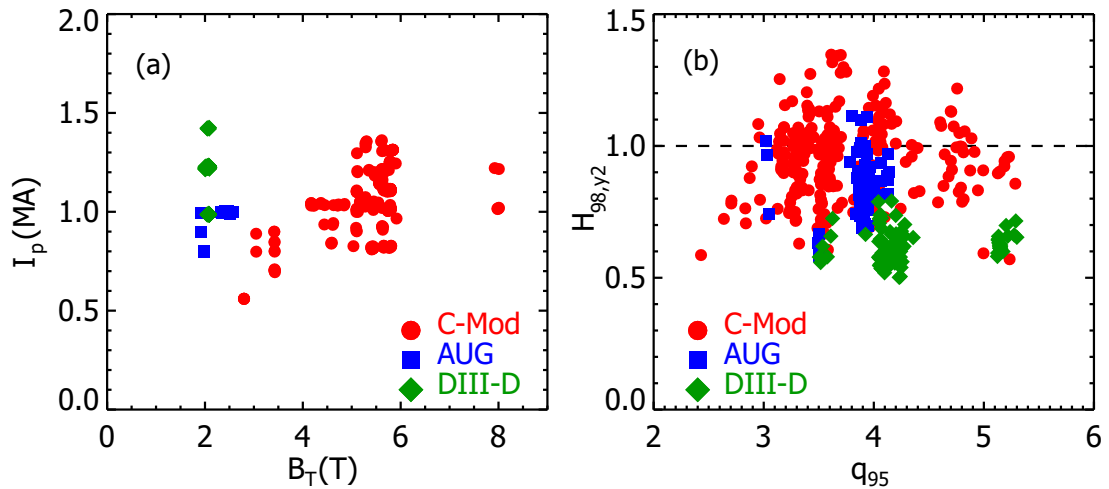
Fig 12

FIG. 12. *Global parameters from a database of C-Mod, AUG and DIII-D I-mode discharges. (a) Plasma current vs toroidal magnetic field (both directions) (b) Normalized energy confinement $H_{98,y2}$ vs q_{95}.*
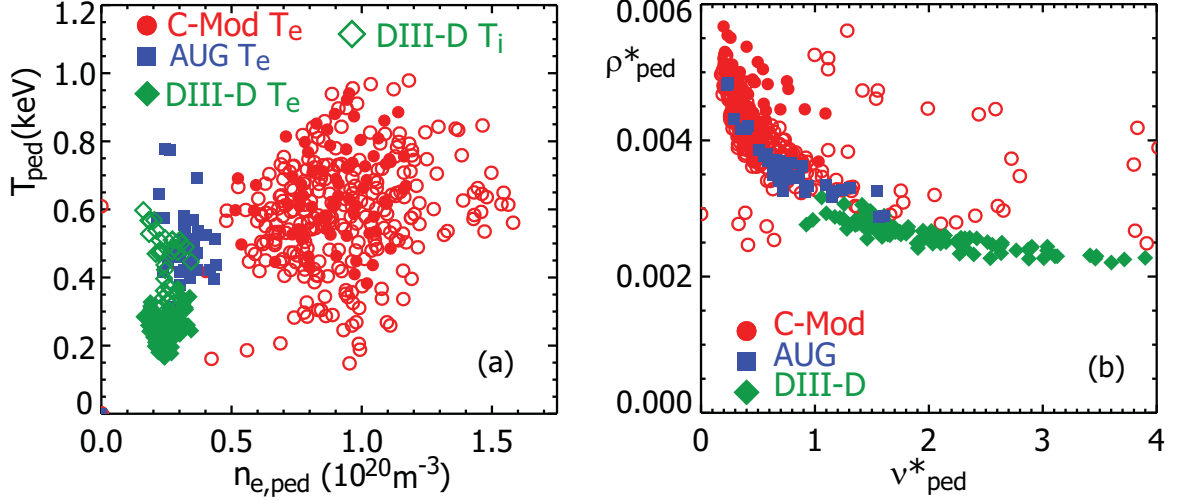
Fig 13

FIG. 13. Parameters at the electron pedestal top from a database of C-Mod, AUG and DIII-D I-mode discharges. (a) T vs n_e at pedestal top.   For C-Mod and AUG, only T_e is shown; the solid C-Mod points are from tanh fits to better resolved pedestal profile data.   For DIII-D, solid diamonds are from fits to T_e pedestals and open diamonds are T_i at the same radial location, where available.   (b) Normalized ion gyroradius ρ^* vs ν^*, computed using $T_{e,ped}$.
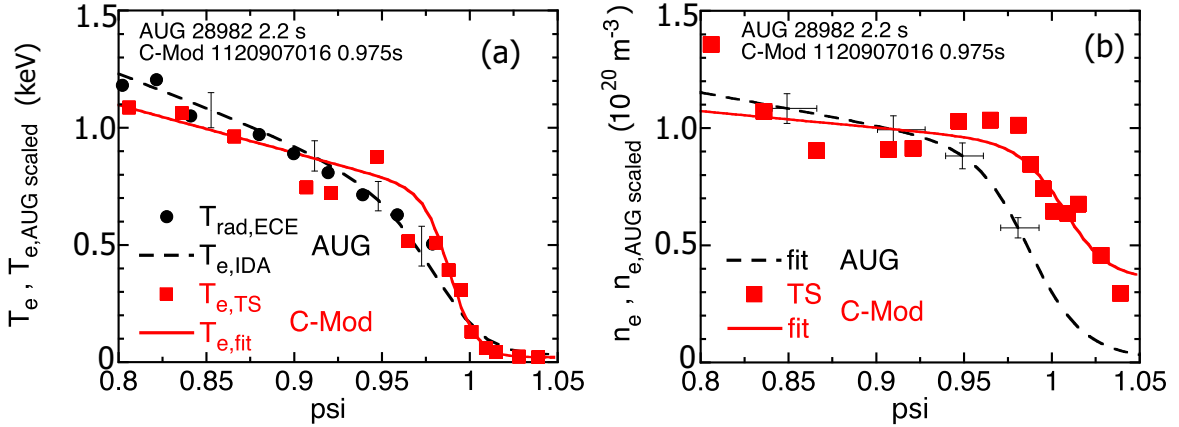
Fig 14

FIG. 14. Pedestal profiles of (a) electron temperature and (b) density in I-mode for a pair of I-mode discharges on C-Mod and AUG. AUG profiles have been scaled by $R_{C-Mod}/R_{AUG}^{-0.5}$ for T_e and R^{-2} for n_e. T_e pedestal profiles are very similar in height and width, while density is shifted outward for C-Mod.
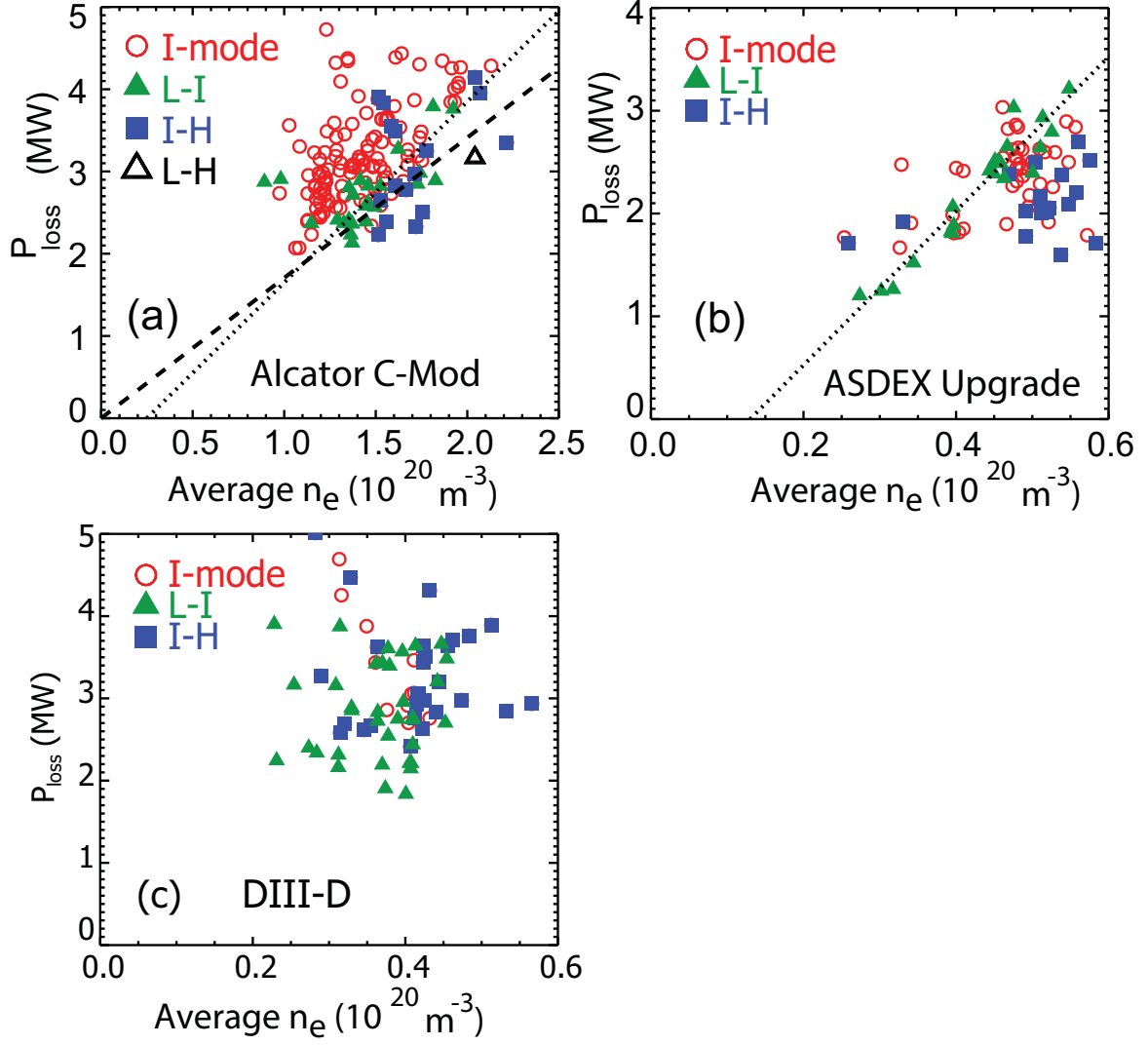
Fig 15

FIG. 15. *Loss power vs line average n_e for I-modes (red circles), L-I transitions (green triangles), and I-H transitions (blue squares), for (a) Alcator C-Mod (5-6 T, 1-1.1 MA, also including an example of a direct L-H transition, black open triangle) (b) ASDEX Upgrade (1.9-2.5 T, 0.8-1.0 MA) (c) DIII-D (2.05 T, 1.2 MA).*
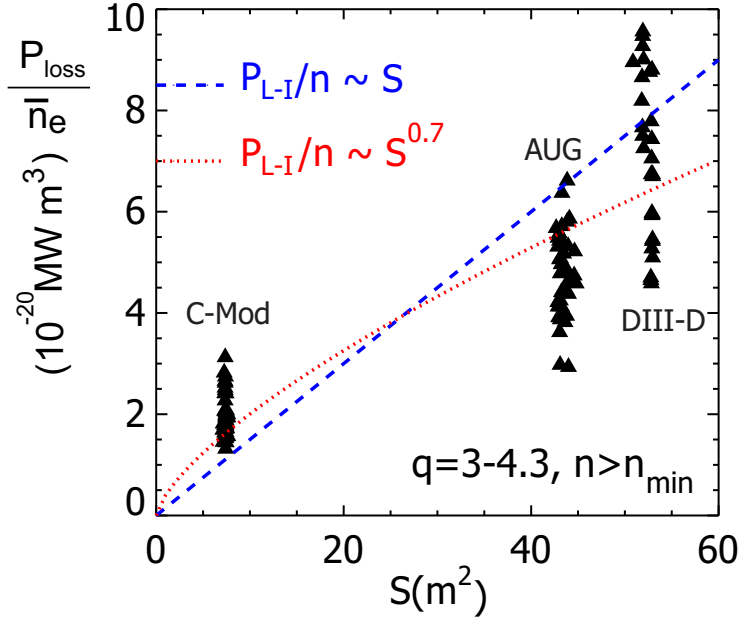
Fig 16

FIG. 16.   *Size scaling of normalized L-I threshold power $P(L-I)/\bar{n}_e$ vs plasma surface area S. While there is considerable scatter in this parameter, the scaling with S appears at most linear and perhaps weaker; the red dotted curve shows $S^{0.7}$.*
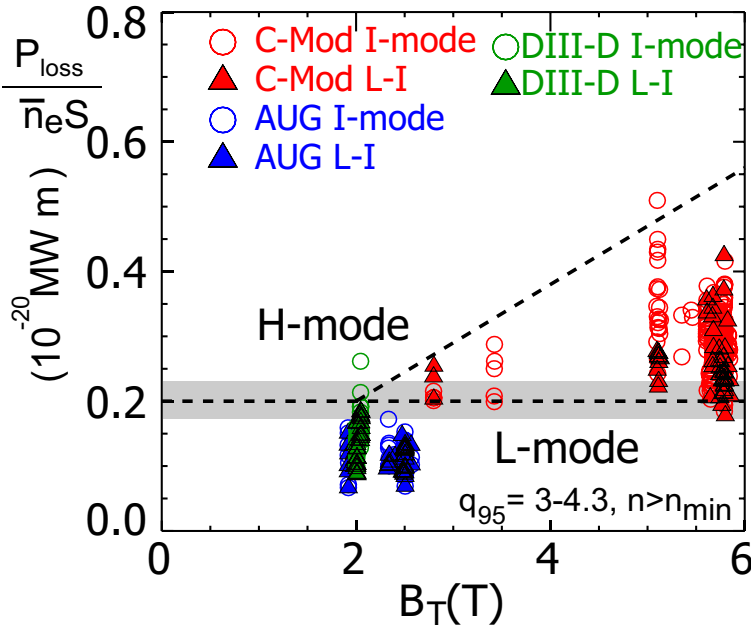
Fig 17

FIG. 17: *Normalized power $P_{loss}/\bar{n}_e S$, vs B_T. Solid triangles are L-I transitions, while open circles are I-modes. Constant and linear magnetic field scalings are shown for reference (dashed lines).*

References

[1] WHYTE D. G., HUBBARD A. E., HUGHES J.W. *et al* 2010 Nuclear Fusion **50** 105005.

[2] BEURSKENS M. A. *et al* 2014 Nucl. Fusion **54** 043001.

[3] WALK J.R. *et al* 2014 Phys. Plasmas **21** 056103.

[4] LOARTE A. *et al*   2014 Nucl. Fusion **54** 033007.

[5] BURRELL K.H. *et al* 2013 Nucl. Fusion **53** 073038.

[6] RYTER F. *et al* (for the ASDEX Upgrade Team), 2011 38th EPS Conference on Plasma Physics (Strasbourg, June 2011), Europhysics Conference Abstracts **35G**, P5.112.

[7] MARINONI A. *et al* 2015 Nucl. Fusion **55** 093019.

[8] HUBBARD A. E. *et al* 2011 Phys. Plasmas **18** 056115.

[9] HUBBARD A.E. *et al*, 2012 Proc. 24th Int. Conf. on Fusion Energy (San Diego, 2012) [EX/1-3] http://www-naweb.iaea.org/napc/physics/FEC/FEC2012/index.htm.

[10] THEILER C., CHURCHILL R.M. *et al* 2014 Nuclear Fusion **54** 083017.

[11] WALK, J.R., Ph.D. Thesis, Massachusetts Institute of Technology 2014.

[12] ITER Physics Basis Expert Groups on Confinement and Transport and Confinement Modelling and Database, ITER Physics Basis Editors 1999 Nucl. Fusion 39 21751999 Nucl.Fusion **39** 2175.

[13] RICE J.E. *et al* 2015 Nucl. Fusion **55** 033014.

[14] WHITE A.E. *et al* 2011 Nuclear Fusion, **51** 113005.

[15] DOMINGUEZ A. Ph.D. Thesis, Physics Department, Massachusetts Institute of Technology (2012).

[16] CZIEGLER I. *et al* 2013 Phys. Plasmas **20** 055904.

[17] WHITE A.E. *et al* 2014 Nucl. Fusion **54** 083019.

[18] WHITE A. E., HOWARD N. T., CREELY A. J. *et al* 2015 Phys. Plasmas **22**, 056109.

[19] VIEZZER E. *et al* 2013 Nucl. Fusion **53** 053005.

[20] HAPPEL T. *et al* "*Turbulence intermittency in the confinement region of I-mode plasmas in the ASDEX Upgrade tokamak*".   Nucl. Fusion, in press.

[21] DA GRACA S. *et al* 2007 Plasma Phys. Control. Fusion **49** 1849–1872.

[22] MANZ P., LAUBER P., NIKLOAEVA V.E. *et al* 2015 Nucl. Fusion **55**, 083004.

[23] PEEBLES, W. A. *et al* 2010 Rev. Sci. Instrum. **81** 10D902.

[24] WILSON H. R., SNYDER P. B., HUYSMAN, G. T. A. and MILLER R. L. 2002 Phys. Plasmas **9**, 1277.

[25] SNYDER P. *et al* 2011 Nucl. Fusion **51** 103016.

[26] OYAMA N. *et al* 2006 Plasma Physics and Controlled Fusion **48**, 5A, A171.

[27] CONNOR J.W. 1988 Plasma Phys. Control. Fusion **30** 619.

[28] LUCE, T.C. *et al* 2008 Plasma Phys. Control. Fusion **50** 043001.

[29] PETTY C.C. et al 2008 Physics of Plasmas **15**, 080501.

[30] SUTTROP W. *et al*. Fusion Energy 2002 (Proc. 19th Int. Conf. Lyon, 2002) (Vienna: IAEA) CD-ROM file and

http://www.iaea.org/programmes/ripc/physics/fec2002/html/fec2002.htm   Vol.   IAEA-CSP-19/CD (2003), IAEA-CN-94/EX/P5-07.

[31] RATHGEBER S. K. *et al* 2013 Plasma Phys. Control. Fusion **55** 025004.

[32] MOSSESSIAN D. *et al* 2003 Phys. Plasmas **10** 1720.

[33] MADDISON G.P. *et al* 2009 Nucl. Fusion **49** 125004.

[34] HUBBARD A.E. *et al* 2012 Nucl. Fusion **52** 114009.

[35] GOHIL P. *et al* 2008 *J. Physics: Conf Series*. **123** 012017.

[36] MARTIN,Y., TAKIZUKA T. *et al*, 2008 *J. Physics: Conf Series*. **123** 012033.

[37] LABOMBARD, B. *et al* 2015 Nucl. Fusion **55** 053020.

[38] SORBOM, B. *et al* 2015 Fusion Engineering and Design **100** 378.